International Journal of Trend in Scientific Research and Development (IJTSRD)
Volume 9 Issue 1, Jan-Feb 2025 Available Online: www.ijtsrd.com e-ISSN: 2456 – 6470

Characterization of the TCO Layer on a Glass Surface for Photovoltaic different Generation Applications

Sneha Bharti[1], Umakant Prasad[2]

[1]Research Scholar, University Department of Physics, T.M.B.U. Bhagalpur, Bihar, India
[2]Retd. Associate Professor, Department of Physics, T.N.B. College Bhagalpur, Bihar, India

ABSTRACT

In the dynamic field of photovoltaic technology, the search for efficiency and sustainability has led to continuous innovation, which has shaped the landscape of solar energy solutions. One of the key elements affecting the efficiency of second and third generation photovoltaic cells is the presence of transparent conductive oxide (TCO) layers, which are key elements affecting the efficiency and durability of solar panels, especially for DSSC, CdTe, CIGS (copper indium gallium diselenide) or organic, perovskite and quantum dots. TCO with low electrical resistance, high mobility and high transmittance in the VIS-NIR region is particularly important in DSSC, CIGS and CdTe solar cells, serving as a window and electron transport layer. This layer must form an ohmic contact with adjacent layers, usually a buffer layer (such as CdS or ZnS), to ensure efficient charge collection. In addition it ensures protection against oxidation and moisture, which is particularly important when transporting the active cell structure to further process steps such as lamination, which ensures the final seal. Transparent conductive oxide layers, which typically include options such as indium tin oxide (ITO) or fluorine-doped tin oxide (FTO), serve a dual purpose in photovoltaic applications. Mainly located as the topmost layer of solar cells, TCOs play a key role in transmitting sunlight while facilitating the efficient collection and transport of generated electrical charges. As the global demand for clean energy grows and the photovoltaic industry develops rapidly, understanding the differential contribution of TCO layers becomes particularly important, especially in the context of using PV modules as building-integrated elements (BIPV). The use of transparent or semi-transparent modules allows the use of building glazing, including windows and skylights. In addition, given the dominant position of the Asian market in the production of silicon-based cells and modules, the European market is intensifying work aimed at finding a competitive PV technology. In this context, thin-film, organic modules could prove to be competitive. To this end, in this work, we focused on the electrical parameters of two different thicknesses of a transparent FTO layer. First, the influence of the FTO layer thickness on transmittance over a wide range was verified. Next, the chemical composition was determined, and key electrical parameters, including carrier mobility, resistivity, and Hall coefficient, were quantified.

How to cite this paper: Sneha Bharti | Umakant Prasad "Characterization of the TCO Layer on a Glass Surface for Photovoltaic different Generation Applications" Published in International Journal of Trend in Scientific Research and Development (ijtsrd), ISSN: 2456-6470, Volume-9 | Issue-1, February 2025, pp.1090-1099, URL: www.ijtsrd.com/papers/ijtsrd76188.pdf

IJTSRD76188

KEYWORDS: *transparent conductive layer; transparent electrode; transparent photovoltaic; transparent BIPV; TCO etc*

1. INTRODUCTION

The use of renewable energy sources is becoming a social norm today. The most popular alternative energy sources include hydropower, biofuels, solar energy, wind power, biomass, and geothermal energy. Among these, solar energy is the most reliable, least expensive, and easiest to use [1]. Various types of solar cells have been developed, including crystalline silicon cells (c-Si), amorphous silicon cells (a-Si), dye-sensitized solar cells (DSSCs), hybrid solar cells [2-4], nanocrystalline solar cells, multijunction SCs,

perovskite SCs, organic SCs, photoelectrochemical cells (PECs), plasmonic SCs, quantum dot SCs (QDSCs), multilayer SCs with gradient band gaps, and semiconductor SCs [5,6]. The physical basis and photovoltaic capabilities of nanowire-IBSCs based on dilute III-V nitride compounds are discussed: these photovoltaic devices promise to overcome many of the limitations encountered to date in the practical implementation of IBSCs based on QD III-V or III-planar NV heterostructures [7]. Organic SCs are increasingly being recognized due to their intrinsic properties, such as light weight, mechanical flexibility and transparency, as well as low production costs. The cSi-based SC cell showed a high efficiency of 27.3% (LONGi) for the heterojunction back-contact (HBC) architecture, improving the previous world record of 27.09%, also set by LONGi at the end of last year [8]. It is worth noting that the presented HBC architecture reduces the dependence on conventional indium-based transparent conductive oxide (ITO). In this context, the research on thin, low-resistance and high-quality FTO layers presented in this work is important. It is well known that an effective way to ensure low reflectance for heterojunction cells is the deposition of transparent conductive oxide (TCO) layers on c-Si substrate [9].

All optically transparent and electrically conductive oxides (TCOs) are binary or ternary compounds containing one or two metallic elements. Their resistivity can be as low as 10–4 Ω, and their extinction coefficient k in the optical visible range (VIS) can be less than 0.0001 due to their wide optical band gap (Eg), which can be larger than 3 eV. This combination of conductivity and transparency is usually impossible in intrinsic stoichiometric oxides. It is achieved by producing them with nonstoichiometric state or by introducing suitable blends [9,10]. The potential and actual application of TOC thin films is in transparent electrodes for photovoltaic cells [11]. Indium tin oxide (ITO) is currently the best TCO electrode material because it has very high transmission (>80%), high conductivity (104 $\Omega^{-1}cm^{-1}$), low refractive index, low light absorption, high strength and stability [12]. Some of the most commonly used semiconductor TCO materials for photovoltaic applications are oxide-doped materials, such as indium-doped tin oxide (ITO), Al-doped zinc oxide (AZO), F-doped tin oxide (FTO), boron-doped zinc oxide and zinc doped with Ga (GZO) [13–15]. In this section, some of their important parameters will be re-introduced. described the deposition of ZnO:Al thin films by DC sputtering on Al_2O_3 (sapphire) oriented monocrystalline substrate (00.1) at high temperature (>350 ◦C), using a low-cost and ultra-high density composite ceramic target produced by pressureless (non-pressure) casting of ZnO-Al_2O_3 (AZO) powder [16]. Thin films of amorphous indium-zinc oxide (IZO) were prepared on glass substrate by direct current magnetron sputtering at room temperature [17]. In the paper, the results show that Al-doped SnO_2 has a p-type conductivity characteristic and its band gap is reduced compared with undoped SnO_2, and the accompanying oxygen vacancies can introduce localized gap states below the conductivity band and lead to a change in the conductivity character from p-type to n-type in Al-doped SnO_2 [18]. The thermal and chemical instability and low surface energy of ITO limit its widespread use [19,20]. The disadvantage of using ITO is the scarcity of indium resources, which is expected to soon increase market prices and reduce ITO supply [21,22]. The brittleness of ITO foil severely limits its use in flexible applications [23,24]. In TCO, the performance of alumina zinc oxide (AZO) is considered to be comparable to ITO and FTO, with other advantages [25], such as low toxicity, low cost, and simple production methods. However, grain boundaries and electron scattering have reduced the mobility of TCO carriers, resulting in an impact on the performance of these materials [26]. One of the main disadvantages of TCO glasses is that they are brittle, cannot withstand high temperatures, and are not suitable for all pH levels [27].

ZnO is of great interest in large-area optoelectronic devices, such as transparent conductive oxides (TCOs), due to its good optical properties. Jung et al. (2019) deposited thin films of quaternary ZnO on soda-lime glass substrates using Mg and group III elements such as Al, Ga, and In to improve optical and electrical properties [28]. However, many studies have been conducted to improve the properties of ZnO by co-doping it with various elements. ZnO doped with group III elements is a good alternative to ITO as it shows good optical transparency in the visible wavelength range and higher conductivity than ITO [29]. In particular, both electrical and optical properties of TCO can be improved by double doping with Mg and group III elements such as Ga, Al and In. Tian et al investigated thin films of ZnO doped with Mg and Ga (MGZO) and observed a wide optical bandgap energy of 3.66 eV and low resistivity of 6.27×10^{-4} Ω [30]. ZnO films doped with Al are a good alternative to ITO due to their superior electro-optical properties [31]. In the study of Saarenpaa et al, Al-doped ZnO films showed better photocatalytic performance than undoped ZnO films [32]. Pure ZnO and Ce-doped ZnO nanoparticles were synthesized by sol-gel coprecipitation method to investigate the temperature-dependent photoluminescence properties

of Ce-doped ZnO nanoparticles. Kumawat et al. analyzed the importance of microstrain in affecting the band gap and photoluminescence (PL) intensity of ZnO thin films [33] doped with Ce on spin-deposited glass substrates using the sol-gel method [34]. Recently, ZnO films doped with different elements have attracted great interest because they can significantly improve the photocatalytic performance compared with single metal-doped ZnO photocatalysts. Therefore, scientists have investigated Al and rare earth-doped ZnO materials due to the mentioned properties of Al and rare earth elements. ZnO doped with Gd and As [35], AZO doped with Eu3+ [36], AZO doped with Sm+3 [37], ZnO doped with Y/Al [38], ZnO doped with Al and/or Ho [39], Ce and Al doped with ZnO [40], and Pr doped with Al:ZnO [41] and Zn(Al,Ce)O nanoparticles [42].

Fluoride-doped SnO2 (FTO) films are semiconductor materials with wide bandgaps (e.g., =3.65 to 4.25 eV) due to their optical transmittance in the visible region [43]. In addition, due to their resistivity, FTO is currently available for practical application. The conductivity of transparent conductive materials is an effective solution [44,45]. Li et al. found that ZnO nanorods on annealed AZO/FTO film exhibit more dense distribution and better orientation than those on FTO glass and unannealed AZO/FTO films. As a result, the annealed AZO/FTO film coated with ZnO nanorods showed superhydrophobicity, high transparency and low visible reflectance, and had the lowest surface resistance of 4.0 Ω/kW, suggesting good electrical conductivity [46]. Li et al. In the study of, transparent conductive layers of ITO and FTO layers with the same sheet resistance were used. PSCs with ITO-coated glass achieved a conversion efficiency of 10.8%, which was higher than that of FTO (9.0%). PSCs with ITO-coated glass substrates have lower resistance in series and parallel connections than PSCs with ITO-coated glass substrates, PSCs with ITO-coated glass substrates have higher transmittance than PSCs with ITO-coated glass substrates, and PSCs with ITO-coated glass substrates can achieve higher IPCE [47]. Mishima et al. investigated the influence of optical properties and surface morphology on the short-circuit current density (JSC) of tin fluoride (FTO)-coated glass substrates for producing perovskite solar cells (PVSCs). Compared to PVSCs on commercially available FTO substrates, PVSCs on our FTO substrate showed an increase in Jsc by 1.4-1.6 mA/cm2. This is not only due to the low absorption of the FTO substrate but also due to the suppression of reflection loss due to the light-trapping effect on the textured surface [48]. Shibayama et al. wrote in their study that proper selection of nanoparticles has proven to be crucial for tuning the properties of F:SnO2 (FTO) nanocomposites. This paper establishes guidelines for the fabrication of FTO and other transparent conductive oxide (TCO) nanocomposites as promising solar cell electrodes with tunable structural, electrical and optical properties [49]. FTO films are mainly prepared by pulsed laser, spray painting and chemical vapor deposition (CVD). When the amount of SnF_2 was 10 wt% and the substrate temperature was 300 ◦C, the resistivity and light transmittance of the film reached 5×10^{-4} Ω.cm and 87%, respectively [50]. However, the resistivity of FTO films prepared by spraying can reach 6×10^{-4} Ω.cm [51]. AFM was used to study the surface morphology of various layers on ITO and FTO. The surface of FTO was much rougher than that of ITO, and the root mean square roughness (RRMS) was 0.63 nm for ITO and 16.0 nm for FTO [52].

Alternative materials and processing technologies have been proposed that can lead to similar PCEs, leading to the development of a second generation of photovoltaic cells, mainly comprised of thin film photovoltaic cells (TFPVs) [53]. Thin films have the advantage of reducing the amount of semiconductors used to fabricate photovoltaic cells, reducing the cost by more than half in many cases [54]. Among the best-known technologies for third-generation solar cells, dye-sensitized solar cells (DSSCs) have emerged when hybrid and highly abundant materials are chosen as the main components [55]. In this work, we compare two FTO layers with different thicknesses made by standard commercial pyrolytic processes to show the applicability of the layers in areas that require specific electrical and optical parameters, such as PV or transparent electronics. The utility of the characterization method for different thicknesses of the TCO layer was confirmed, furthermore, from the measurements made, the optimum thickness of the layer can be selected taking into account the layer quality and the electrical and optical parameters.

2. Materials & Methods

Sample Preparation

Two FTO layers formed by pyrolytic process on glass substrate were investigated to find out their chemical, electrical and optical parameters. The first coating with a thickness of 540 nm was prepared on 3.2 mm glass (sample 1). The second sample had a 340 nm TCO coating on a 3.2 mm glass substrate (sample 2). Both samples were measured by SEM-EDS and a Hall effect measurement analyzer (HCS10, Linseis GmbH, Hitachi, Japan) to find out their chemical composition and electrical parameters, especially charge carrier concentrations and mobility. For the

substrate commercial (DiGlasco Glass Tech), 3.2 mm tempered clear glass with Si edge grinding was used. Local curvature less than 2‰ and transmittance of 89% were specified. Before deposition, the process glass substrate was cleaned in an ultrasonic cleaner using acetone for 10 min and then cleaned in isopropanol for 15 min. After that, the substrate was dried using nitrogen blow through. The FTO layers were formed using a standard ultrasonic 1.62 MHz spray pyrolysis process in a furnace chamber heated to 480 ◦C and tin(IV) chloride pentahydrate with ammonium fluoride as the precursor. The spray nozzle was placed 15 cm above the glass substrate, and the scan speed was set to 1.5 cm/s for sample 1 and 1 cm/s for sample 2. Before spraying, the substrate was heated to reach a temperature of 480 ◦C and then stabilized for 15 min. The original dimensions of the measured samples were 300 × 300 mm^2. Since the sample holder is suitable for 10 × 10 mm^2, the glass was cut to that dimension and cleaned of dust by a dry nitrogen stream before any measurements. Since the substrate glass was tempered for cutting, a laser machine with a 10 picosecond, 1064 nm wavelength was used. They were not cleaned in an ultrasonic bath to avoid damaging the coatings. The samples prepared in the manner described above were then placed in the sample holder (see Figure 1) and transferred to the measurement chamber in the HCS10 device and to the secondary electron microscope (SEM) system equipped with EDS. The scanning electron microscope (SEM) Hitachi Regulus 8230 was used for sample imaging. The SEM was equipped with a cold field emission gun (CFE) and in-column), a secondary electron SE detector, two in-lens SE detectors and a backscatter detector BSE detector as well as energy dispersive spectroscopy (EDS) detectors (Thermo Scientific, Rzeszow, Poland) with a detector surface of 60 mm2 and a resolution of 129 eV specified for the manganese K line. Images were registered at accelerating voltages between 10 and 15 kV and working distances between 2 and 4 mm.

Figure 1. A sample with dimensions of 10×10 mm^2 was mounted in the sample holder.

3. Results and Discussion:

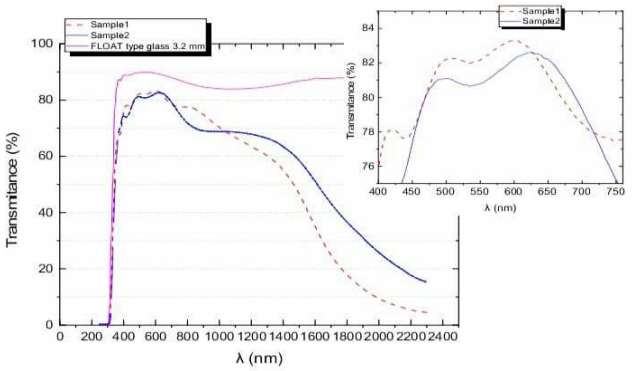

Figure 2: Results of optical measurements on samples 1 and 2 and substrates: standard float glass and highly transparent optical white glass for comparison

The transmission of the samples (samples 1 and 2) with FTO layers showed a significant decrease compared to the neat substrate (float 3.2 mm) especially in the IR range. In addition, for a rougher sample (sample 1), higher absorption was observed in the IR region. This is due to free carrier absorption and may also be related to the chemical composition or surface roughness. The specific composition of FTO, including the ratio of tin to fluorine and the doping level, can affect its optical properties. In some cases, variations in composition can lead to increased absorption in the IR region. Since there were no significant differences in the spectra of the measured samples, it can be concluded that the chemical composition of both samples was the same. In addition, it can be concluded from the optical measurements that the surface morphology is the same. In addition, the difference in thickness, namely 200 nm, is evident in the optical spectrum, indicating that spectroscopic measurements are useful for determining the difference in thickness between layers. The average transmittance of the VIS region (300-880 nm) calculated for samples 1 and 2 are 73.4 and 71.02, respectively, which is unsatisfactory for transparent conductive layers for electronics applications (the expected transmittance should be in the range of 80%). The low transmittance may be associated with the low quality of the layer and is also related to the substrate (float glass). According to [56,57], the average transmittance in the VIS region should not be much affected by different fluorine doping levels. From the optical spectrum of the VIS region (Figure 2 entry), very few fringes can be observed, which may be associated with low fluoride concentration. From the Tauc's plot (Figure 3), the direct transition and energy band gap values were found to be approximately equal to 3.59 eV and 3.49 eV for samples 1 and 2, respectively, which is consistent with the FTO optical Eg values in the

literature. The value obtained is slightly lower than that of undoped tin oxide material, which is about 3.7 eV. According to the Burstein-Moss effect, the energy of the band gap for doped metal oxide layers should be higher than that of undoped metal oxide layers. This can be explained by the fact that the energy gap between the valence band and the lowest vacant state in the conduction band is found to increase due to the filling of low-lying energy levels in the conduction band, which is caused by the increase in carrier concentration. For very thin films of a few hundred nanometers (340-540 nm for the analyzed samples), the shift in the bandgap may be a result of ferroic strain or free carrier concentration. It is well known that for different thicknesses of FTO layer, different surface morphologies can be obtained [58]. For a film with higher thickness (1.38 mm), almost full of large grains was observed. For films with thicknesses between 0.92 and 1.01 mm, the grains were found to be uniform in size and clustered in a cubic shape. When the layer thickness is reduced to 0.72 and 0.84 mm, grains with regular rectangular shapes clustered on the surface. For films with other thicknesses, the morphology is characterized by needle-shaped grains.

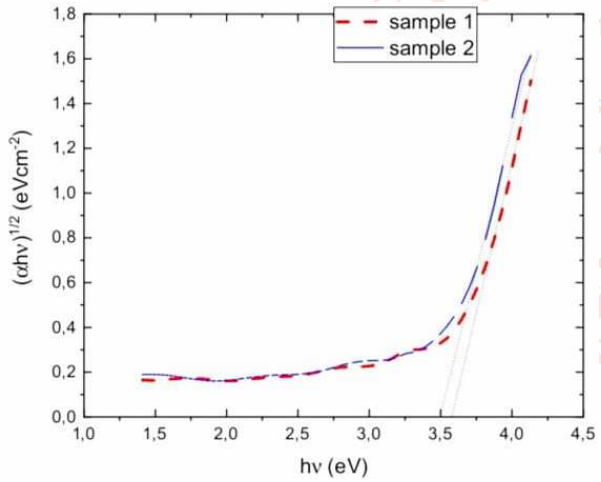

Figure 3: Tauc plot of the allowed direct FTO transition.

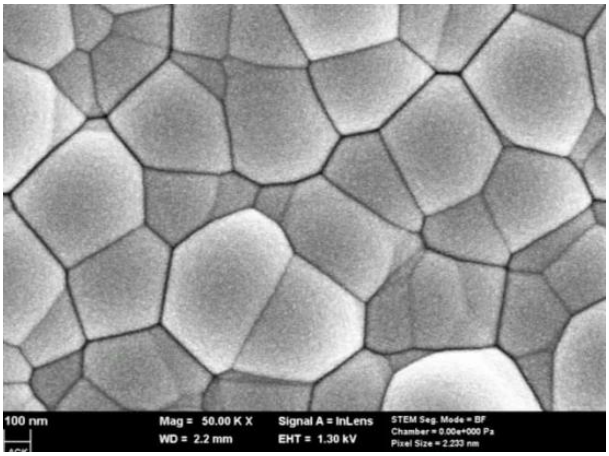

Figure 4: SEM image of the surface of sample 1.

The chemical composition was verified using a SEM Hitachi Regulus 8230 instrument equipped with an energy dispersive spectroscopy (EDS) detector. Two pieces of glass containing an FTO layer were placed inside the SEM chamber, and for both samples, measurements were performed on two sides: an FTO coating and a glass-bearing electron source. The elemental composition was determined at an accelerating voltage of 15 kV and a working distance set at 2.2 mm. Since the FTO layer is conductive, it was easy to obtain a high-resolution image; additionally, the applied high voltage did not damage the surface. The situation was completely different when measurements were performed from the glass side. A high charge accumulation effect was observed, which significantly affected the collected data. A clear signature of the atoms in the FTO layer is visible, namely, Sn (La 3.443) and F (Ka 0.677). Since the layer is relatively thin (540 nm), a clear signature of atoms from the glass substrate is noticeable (Si, Na, Ca). For a thin FTO layer, one might expect to see a significantly higher signal from the glass. Fluorine is present in the FTO coating; however, a small content (<0.1% by weight) is present. Its presence is confirmed by a visible signal in the spectrum (Figures 5 and 6). The relatively high ratio of the oxygen peak (Ka 0.525) to the silicon peak (Ka 1.739) suggested that the electron beam was less likely to penetrate the glass surface, and most of the observed oxygen was present in the FTO film.

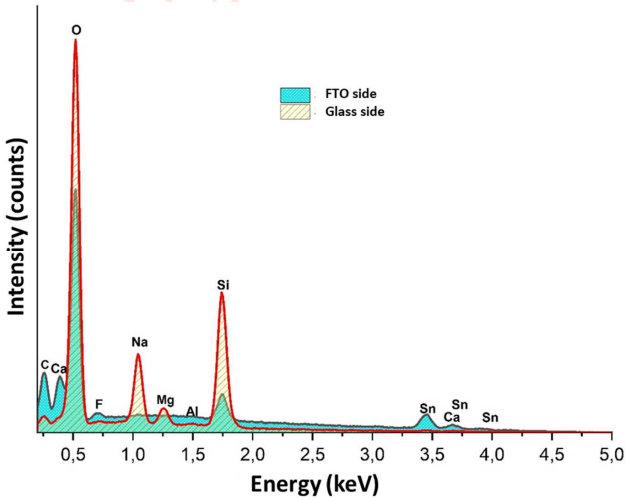

Figure 5: EDS spectrum collected on sample 1 (FTO 540 nm) for both sides (FTO and the back glass on top).

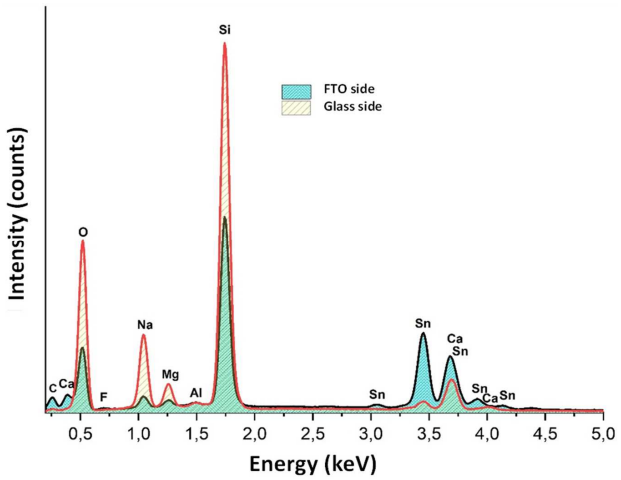

Figure 6: EDS spectrum collected on sample 2 (FTO 340 nm) for both sides (FTO and the back glass on top).

The determined Hall parameters are summarized in Table 1 for SAMPLE1 and Table 2 for SAMPLE2. The values presented in both tables were obtained for samples 1 and 2, each of which was taken from a different location (three measurements for each sample are denoted as 1.1, 1.2, and 1.3). Then, the data were averaged (AVG), and the standard deviation (SD) was calculated. As expected, the thicker FTO layer led to a lower sheet resistance of 7.50 and 13.80 Ω−1 for SAMPLE1 and SAMPLE2, respectively. Similar conclusions can also be drawn for the conductivity. At 540 nm, the conductivity of FTO was 2469 Ω^{-1} cm^{-1}, while at 340 nm, it was 2135 Ω^{-1} cm^{-1}. These results indicate that SAMPLE1 performs better electrically. The data obtained showed that the bulk charge carrier concentration (CCC) for SAMPLE2 (−4.45 × 1020 cm^{-3}) was higher than that for SAMPLE1 (−4.02 ×1020 cm^{-3}); however, the sheet CCC for SAMPLE1 (−2.17 × 1020 cm^{-2}) was higher than that for SAMPLE2 (−1.51 × 1020 cm^{-2}). The higher bulk CCC may suggest that the quality of the thin layer is better because the presence of defects and impurities in the material can significantly affect the bulk charge carrier concentration. These defects may act as trap states, affecting the mobility and concentration of charge carriers, which was observed in the case of the measured samples. During the measurement, the HCS10 device measures the Hall coefficient between the BD connection points and then between the AC connection points. These points are labeled on the sample holder (see Figure 1). The final Hall coefficient is then determined by calculating the average value of these two results. As presented in both tables, the coefficient is negative, which means that the majority of carriers in the material are electrons. The last calculated parameter was the mobility. It was significantly higher for the thicker FTO coatings in SAMPLE1 (−38.34 $cm^2V^{-1}s^{-1}$) than in SAMPLE2 (−29.92 $cm^2V^{-1}s^{-1}$). The obtained mobility values are higher than the values reported in [59], where samples were prepared using a similar technique, but with a significantly thicker layer in the range of 1-2 µm. The thinness of the layer may be related to the higher quality of the layer, which reduces the resistance. Thin films can have higher defect density and surface scattering, which can reduce mobility, however, for thicker layers, delocalization can improve mobility to an extent, but very thick films can introduce other issues such as stress or strain, which can also affect mobility. In the present case, one can conclude that the defect concentration is lower in the thicker film.

Table 1: Hall parameters were determined for the SAMPLE1 sample (540 nm of FTO).

SAMPLE1									
Sample ID	Sheet Resistance (Ω^{-1}) ±0.01	Resistivity (Ω cm) ±0.02 × $10^{-0.4}$	Conductivity (Ω^{-1} cm^{-1}) ±0.02 × 10^2	CCC Bulk (cm^{-3}) ±0.05 × 10^{20}	CCC Sheet (cm^{-2}) ±0.05 × 10^{20}	BD Cross Hall Coef. (cm^3 C^{-1}) ±0.01 × 10^{-2}	AC Cross Hall Coef. (cm^3 C^{-1}) ±0.01 × 10^{-2}	Avg. Hall Coef. (cm^3 C^{-1}) ±0.01 × 10^{-2}	Mobility (cm^2 V^{-1} s^{-1}) ±0.01
1.1	7.47	4.03 × 10^{-4}	2480	−4.18 × 10^{20}	−2.26 × 10^{20}	−0.0150	−0.0149	−0.0149	−37.06
1.2	7.50	4.05 × 10^{-4}	2470	−3.91 × 10^{20}	−2.11 × 10^{20}	−0.0161	−0.0159	−0.0160	−39.44
1.3	7.54	4.07 × 10^{-4}	2456	−3.98 × 10^{20}	−2.15 × 10^{20}	−0.0158	−0.0156	−0.0157	−38.54
AVG	7.50	4.05 × 10^{-4}	2469	−4.02 × 10^{20}	−2.17 × 10^{20}	−0.0156	−0.0155	−0.0155	−38.34
SD	0.04	0.02 × 10^{-4}	12	0.14 × 10^{20}	0.08 × 10^{20}	0.0006	0.0005	0.0005	1.20

Table 2: The Hall parameters were determined for sample 2 (with a wavelength of 340 nm for FTO).

SAMPLE2									
Sample ID	Sheet Resistance (Ω^{-1}) ±0.01	Resistivity (Ω cm) ±0.02 × $10^{-0.4}$	Conductivity (Ω^{-1} cm^{-1}) ±0.02 × 10^2	CCC Bulk (cm^{-3}) ±0.05 × 10^{20}	CCC Sheet (cm^{-2}) ±0.05 × 10^{20}	BD Cross Hall Coef. (cm^3 C^{-1}) ±0.01 × 10^{-2}	AC Cross Hall Coef. (cm^3 C^{-1}) ±0.01 × 10^{-2}	Avg. Hall Coef. (cm^3 C^{-1}) ±0.01 × 10^{-2}	Mobility (cm^2 V^{-1} s^{-1}) ±0.01
2.1	13.79	4.69 × 10^{-4}	2133	−4.34 × 10^{20}	−1.48 × 10^{20}	−0.0144	−0.0144	−0.0144	−30.67
2.2	14.44	4.91 × 10^{-4}	2037	−4.35 × 10^{20}	−1.48 × 10^{20}	−0.0143	−0.0144	−0.0143	−29.23
2.3	13.16	4.47 × 10^{-4}	2235	−4.67 × 10^{20}	−1.59 × 10^{20}	−0.0134	−0.0134	−0.0134	−29.85
AVG	13.80	4.69 × 10^{-4}	2135	−4.45 × 10^{20}	−1.51 × 10^{20}	−0.0140	−0.0141	−0.0140	−29.92
SD	0.64	0.22 × 10^{-4}	99	0.19 × 10^{20}	0.07 × 10^{20}	0.0006	0.0006	0.0006	0.72

4. Conclusions

Two TCO samples were investigated by optical spectroscopy, SEM-EDS and Hall measurements. The first sample was made of a float glass substrate and a 540 nm FTO coating (SAMPLE1), while the second sample was also prepared on a similar substrate, but the FTO layer thickness was 340 nm (SAMPLE2). No significant differences were found by

spectroscopic characterization. The similar spectra for both samples suggested very similar chemical and electrical parameters. If it were possible to easily determine the basic parameters using simple and quick spectrophotometric measurements, this method could be widely used in quality control processes at the production level. This hypothesis was not supported by further studies using EDS and Hall. First, SEM with EDS demonstrated that for such a thin layer of FTO, unambiguous determination of the chemical composition of specific atoms is difficult. Additionally, the significant effect of the substrate may disrupt the results. As expected, the thicker layer had better electrical parameters, such as sheet resistance or conductivity. Additionally, the mobility of charge carriers was the highest for that sample. From the optical spectrum in the VIS region, the bandgap values were found to be similar for both samples. In both cases, the Hall coefficient was negative, which indicated that electrons are the majority carriers in that material. The sheet charge carrier concentration was higher for SAMPLE1, but surprisingly, the bulk charge carrier concentration was higher for the SAMPLE2 sample. This may be due to the relatively low thickness of the coating, which introduces quantum effects on the surface. In this work, we show that a thicker FTO layer formed using the pyrolysis process (540 nm) is more suitable for PV and transparent electronic applications due to its higher mobility and lower resistivity. Moreover, a thicker layer does not reduce the transmittance in the VIS I IR region, which is important for the III generation of photovoltaic devices.

5. References

[1] Ciuła, J.; Generowicz, A.; Gronba-Chyła, A.; Wiewiórska, I.; Kwa´snicki, P.; Cygnar, M. Analysis of the Efficiency of Landfill Gas Treatment for Power Generation in a Cogeneration System in Terms of the European Green Deal. *Sustainability* 2024, *16*, 1479. [CrossRef]

[2] Sciuto, G.L.; Capizzi, G.; Shikler, R.; Napoli, C. Organic solar cells defects classification by using a new feature extraction algorithm and an EBNN with an innovative pruning algorithm. *Int. J. Intell. Syst.* 2021, *36*, 2443–2464. [CrossRef]

[3] Sciuto, G.L.; Coco, S. A 3D finite element model of degradation phenomena in organic solar devices affected by oxidation. *Int. J. Energy Environ. Eng.* 2020, *11*, 431–437. [CrossRef]

[4] Barbusi´nski, K.; Kwa´snicki, P.; Gronba-Chyła, A.; Generowicz, A.; Ciuła, J.; Szel ˛ag, B.; Fatone, F.; Makara, A.; Kowalski, Z. Influence of Environmental Conditions on the Electrical Parameters of Side Connectors in Glass–Glass Photovoltaic Modules. *Energies* 2024, *17*, 680. [CrossRef]

[5] Sciuto, G.L.; Napoli, C.; Capizzi, G.; Shikler, R. Organic solar cells defects detection by means of an elliptical basis neural network and a new feature extraction technique. *Optik* 2019, *194*, 163038. [CrossRef]

[6] Kwa´snicki, P.; Gronba-Chyła, A.; Generowicz, A.; Ciuła, J.; Wiewiórska, I.; Gaska, K. Alternative method of making electrical connections in the 1st and 3rd generation modules as an effective way to improve module efficiency and reduce production costs. *Arch. Thermodyn.* 2023, *44*, 179–200.[CrossRef]

[7] Prete, P.; Lovergine, N. Dilute nitride III-V nanowires for high-efficiency intermediate-band photovoltaic cells: Materials requirements, self-assembly methods and properties. *Prog. Cryst. Growth Charact. Mater.* 2020, *66*, 100510. [CrossRef]

[8] Ziani, N.; Belkaid, M.S. Computer Modelling Zinc Oxide/Silicon Heterojunction Solar Cells. *J. Nano Electron. Phys.* 2018, *10*, 06002. [CrossRef]

[9] Afre, R.; Sharma, N.; Sharon, M.; Sharon, M. Transparent Conducting Oxide Films for Various Applications: A Review. *Rev. Adv. Mater. Sci.* 2018, *53*, 79–89. [CrossRef]

[10] Yu, L.; O'Donnell, B.; Alet, P.-J.; Cabarrocas, P.R. All-in situ fabrication and characterization of silicon nanowires on TCO/glass substrates for photovoltaic application. *Sol. Energy Mater. Sol. Cells* 2010, *94*, 1855–1859. [CrossRef]

[11] Preeti; Kumar, S. Extraction and analysis of TCO coated glass from waste amorphous silicon thin film solar module. *Sol. Energy Mater. Sol. Cells* 2023, *253*, 112227. [CrossRef]

[12] He, T.; Xie, A.; Reneker, D.H.; Zhu, Y. A tough and high-performance transparent electrode from a scalable and transfer-free method, Wu. *ACS Nano* 2014, *8*, 4782–4789. [CrossRef]

[13] Chiu, H.L.; Hong, K.B.; Huang, K.C.; Lu, T.C. Photonic Crystal Surface Emitting Lasers with Naturally, Formed Periodic ITO Structures. *ACS Photonics* 2019, *6*, 684–690. [CrossRef]

[14] Sima, C.; Grigoriu, C.; Antohe, S. Comparison of the dye-sensitized solar cells performances based on transparent conductive ITO and FTO. *Thin Solid Film.* 2010, *519*, 595–597. [CrossRef]

[15] Sang, B.; Kushiya, K.; Okumura, D.; Yamase, O. Performance improvement of CIGS-based modules by depositing high-quality Ga-doped ZnO windows with magnetron sputtering. *Sol. Energy Mater. Sol. Cells* 2001, *67*, 237–245. [CrossRef]

[16] Miccoli, I.; Spampinato, R.; Marzo, F.; Prete, P.; Lovergine, N. DC-magnetron sputtering of ZnO:Al films on (00.1)Al2O3 substrates from slip-casting sintered ceramic targets. *Appl. Surf. Sci.* 2014, *313*, 418–423. [CrossRef]

[17] Li, G.F.; Zhou, J.; Huang, Y.W.; Yang, M.; Feng, J.H.; Zhang, Q. Indium zinc oxide semiconductor thin films deposited by dc magnetron sputtering at room temperature. *Vacuum* 2010, *85*, 22–25. [CrossRef]

[18] Lai, K.; Sun, Y.; Chen, H.; Zhi, L.; Wei, W. Effect of oxygen vacancy and Al-doping on the electronic and optical properties in SnO2 . *Phys. B Condens. Matter.* 2013, *428*, 48–52. [CrossRef]

[19] Park, J.H.; Buurma, C.; Sivananthan, S.; Kodama, R.; Gao, W.; Gessert, T.A. The effect of postannealing on Indium Tin Oxide thin films by magnetron sputtering method. *Appl. Surf. Sci.* 2014, *307*, 388–392. [CrossRef]

[20] Chavan, G.T.; Kim, Y.; Khokhar, M.Q.; Hussain, S.Q.; Cho, E.-C.; Yi, J.; Ahmad, Z.; Rosaiah, P.; Jeon, C.-W. A Brief Review of Transparent Conducting Oxides (TCO): The Influence of Different Deposition Techniques on the Efficiency of Solar Cells. *Nanomaterials* 2023, *13*, 1226. [CrossRef]

[21] Hussain, S.Q.; Kim, S.; Ahn, S.; Balaji, N.; Lee, Y.; Lee, J.H.; Yi, J. Influence of high work function ITO:Zr films for the barrier height modification in a-Si:H/c-Si heterojunction solar cells. *Sol. Energy Mater. Sol. Cells* 2014, *122*, 130–135. [CrossRef]

[22] Lee, J.Y.; Connor, S.T.; Cui, Y.; Peumans, P. Solution-processed metal nanowire mesh transparent electrodes. *Nano Lett.* 2008, *8*, 689–692. [CrossRef] [PubMed]

[23] Madaria, A.R.; Kumar, A.; Ishikawa, F.N.; Zhou, C. Uniform, highly conductive and patterned transparent films of a percolating silver nanowire network on rigid and flexible substrates using a dry transfer technique. *Nano Res.* 2010, *3*, 564–573. [CrossRef]

[24] Rathmell, A.R.; Bergin, S.M.; Hua, Y.L.; Li, Z.Y.; Wiley, B.J. The growth mechanism of copper nanowires and their properties in flexible, transparent conducting films. *Adv. Mater.* 2010, *22*, 3558–3563. [CrossRef] [PubMed]

[25] Mohl, M.; Dombovari, A.; Vajtai, R.; Ajayan, P.M.; Kordas, K. Self-assembled large scale metal alloy grid patterns as flexible transparent conductive layers. *Sci. Rep.* 2015, *5*, 13710. [CrossRef] [PubMed]

[26] Jung, Y.S.; Park, Y.S.; Kim, K.H.; Lee, W.J. Properties of AZO/Ag/AZO multilayer thin film deposited on polyethersulfone substrate. *Trans. Electr. Electron. Mater.* 2013, *14*, 9–11. [CrossRef]

[27] Rosli, N.N.; Ibrahima, M.A.; Ludin, N.A.; Teridi, M.A.M.; Sopian, K. A review of graphene based transparent conducting films for use in solar photovoltaic applications. *Renew. Sustain. Energy Rev.* 2019, *99*, 83–99. [CrossRef]

[28] Sun, J.; Jasieniak, J.J. Semitransparent solar cells. *Phys. D Aplik. Fiz.* 2017, *50*, 093001. [CrossRef]

[29] Jang, J.S.; Kim, J.; Ghorpade, U.; Shin, H.H.; Gang, M.G.; Park, S.D.; Kim, H.J.; Lee, D.S.; Kim, J.H. Comparison study of ZnO-based quaternary TCO materials for photovoltaic application. *J. Alloys Compd.* 2019, *793*, 499–504. [CrossRef]

[30] Kim, I.Y.; Shin, S.W.; Gang, M.G.; Lee, S.H.; Gurav, K.V.; Patil, P.S.; Yun, J.H.; Lee, J.Y.; Kim, J.H. Comparative study of quaternary Mg and Group III element codoped ZnO thin films with transparent conductive characteristics. *Thin Solid Film.* 2014, *570*, 321–325. [CrossRef]

[31] Karakaya, S.; Kaba, L. Wrinkle type nanostructured of Al-Ce codoped ZnO thin films for photocatalytic applications. *Surf. Interfaces* 2024, *44*, 103655. [CrossRef]

[32] Saarenpaa, H.; Niemi, T.; Tukiainen, A.; Lemmetyinen, H.; Tkachenko, N. Aluminum doped zinc oxide films grown by atomic layer deposition for organic photovoltaic devices. *Sol. Energy Mater. Sol. Cells* 2010, *94*, 1379–1383. [CrossRef]

[33] Gultepe, O.; Atay, F. The effect of Al element on structural, optical, electrical, surface and photocatalytic properties of Solgel derived ZnO films. *Appl. Phys. A* 2022, *128*, 25. [CrossRef]

[34] Kumawat, A.; Sharma, A.; Chattopadhyay, S.; Misra, K.P. Temperature dependent photoluminescence in Sol-gel derived Ce doped ZnO nanoparticles. *Mater. Today Proc.* 2021, *43*, 2965–2969. [CrossRef]

[35] Kumawat, A.; Chattopadhyay, S.; Misra, R.D.K.; Misra, K.P.; Valiyaneerilakkal, U. Significance of microstrain in impacting band gap and photoluminescence behavior of Ce-doped ZnO thin films deposited via sol-gel process. *Phys. Scr.* 2023, *98*, 025816. [CrossRef]

[36] Anand, V.; Sakthivelu, A.; Kumar, K.D.A.; Valanarasu, S.; Ganesh, V.; Shkir, M.; Kathalingam, A.; AlFaify, S. Novel rare earth Gd and Al co-doped ZnO thin films prepared by nebulizer spray method for optoelectronic applications. *Superlattices Microstruct.* 2018, *123*, 311–322. [CrossRef]

[37] Anand, V.; Sakthivelu, A.; Kumar, K.D.A.; Valanarasu, S.; Ganesh, V.; Shkir, M.; AlFaify, S.; Algarni, H. Rare earth Eu3+ codoped AZO thin films prepared by nebulizer spray pyrolysis technique for optoelectronics. *J. Solgel Sci. Technol.* 2018, *86*, 293–304. [CrossRef]

[38] Anand, V.; Sakthivelu, A.; Deva Arun Kumar, K.; Valanarasu, S.; Kathalingam, A.; Ganesh, V.; Shkir, M.; AlFaify, S.; Yahia, I.S. Rare earth Sm3+ codoped AZO thin films for opto-electronic application prepared by spray pyrolysis. *Ceram. Int.* 2018, *44*, 6730–6738. [CrossRef]

[39] Üzar, N.; Algün, G.; Akçay, N.; Akcan, D.; Arda, L. Structural, optical, electrical and humudity sensing properties of (Y/Al) codoped ZnO thin films. *J. Mater. Sci. Mater. Electron.* 2017, *28*, 11861–11870. [CrossRef]

[40] Mereu, R.A.; Mesaros, A.; Vasilescu, M.; Popa, M.; Gabor, M.S.; Ciontea, L.; Petrisor, T. Synthesis and characterization of undoped, Al and/or Ho doped ZnO thin Films. *Ceram. Int.* 2013, *39*, 5535–5543. [CrossRef]

[41] Ahmed, M.A.M.; Meyer, W.E.; Nel, J.M. Effect of (Ce, Al) codoped ZnO thin films on the Schottky diode properties fabricated using the sol-gel spin coating. *Mater. Sci. Semicond. Process.* 2019, *103*, 104612. [CrossRef]

[42] Kumar, K.D.A.; Thomas, R.; Valanarasu, S.; Ganesh, V.; Shkir, M.; AlFaify, S.; Thirumalai, J. Analysis of Pr codoped Al: ZnO thin flms using feasible nebulizer spray technique for optoelectronic technology. *Appl. Phys. A* 2019, *125*, 712. [CrossRef]

[43] Sharma, A.; Kumawat, A.; Chattopadhyay, S.; Khangarot, R.K.; Halder, N.; Misra, R.D.K.; Misra, K.P. Band gap reduction and Zn related defects enhancement in Zn(Al, Ce)O nanoparticles. *Mater. Today Proc.* 2022, *60*, 21–25. [CrossRef]

[44] Kambe, M.; Fukawa, M.; Taneda, N.; Sato, K. Improvement of a-Si solar cell properties by using SnO2 : F TCO films coated with an ultrathin TiO2 layer prepared by APCVD. *Sol. Energy Mater. Sol. Cells* 2006, *90*, 3014–3020. [CrossRef]

[45] Consonni, V.; Rey, G.; Roussel, H.; Doisneau, B.; Blanquet, E.; Bellet, D. Preferential orientation of fluorine-doped SnO2 thin films: The effects of growth temperature. *Acta Mater.* 2013, *61*, 22–31. [CrossRef]

[46] Yu, S.; Li, L.; Lyu, X.; Zhang, W. Preparation and investigation of nanothick FTO/Ag/FTO multilayer transparent electrodes with high figure of merit. *Sci. Rep.* 2016, *6*, 20399. [CrossRef] [PubMed]

[47] Li, B.; Huang, L.; Ren, N.; Kong, X.; Cai, Y.; Zhang, J. Superhydrophobic and anti-reflective ZnO nanorod-coated FTO transparent conductive thin films prepared by a three-step method. *J. Alloys Compd.* 2016, *674*, 368–375. [CrossRef]

[48] Mishima, R.; Hino, M.; Uzu, H.; Meguro, T.; Yamamoto, K. High-current perovskite solar cells fabricated with optically enhanced transparent conductive oxides. *Appl. Phys. Express* 2017, *10*, 062301. [CrossRef]

[49] Shibayama, N.; Fukumoto, S.; Sugita, H.; Kanda, H.; Ito, S. Influence of transparent conductive oxide layer on the inverted perovskite solar cell using PEDOT: PSS for hole transport layer. *Mater. Res. Bull.* 2018, *106*, 433–438. [CrossRef]

[50] Zhang, S.-T.; Foldyna, M.; Roussel, H.; Consonni, V.; Pernot, E.; Schmidt-Mende, L.; Rapenne, L.; Jiménez, C.; Deschanvres, J.-L.; Muñoz-Rojas, D.; et al. Tuning the properties of F:SnO2 (FTO) nanocomposites with S:TiO2 nanoparticles—Promising hazy transparent

electrodes for photovoltaics applications. *J. Mater. Chem. C* 2017, *5*, 91–102. [CrossRef]

[51] Kim, H.; Auyeung, R.C.Y.; Pique, A. Transparent conducting F-doped SnO2 thin films grown by pulsed laser deposition. *Thin Solid Film.* 2008, *516*, 5052–5056. [CrossRef]

[52] Qia, F.; Chu, H.; Xie, Y.; Weng, Z. Recent progress of transparent conductive electrodes in the construction of efficient flexible organic solar cells. *Int. J. Energy Res.* 2022, *46*, 4071–4087. [CrossRef]

[53] Way, A.; Luke, J.; Evans, A.D.; Li, Z.; Kim, J.-S.; Durrant, J.R.; Ka Hin Lee, H.; Tsoi, W.C. Fluorine doped tin oxide as an alternative of indium tin oxide for bottom electrode of semi-transparent organic photovoltaic devices. *AIP Adv.* 2019, *9*, 085220. [CrossRef]

[54] Yang, Z.; Song, J.; Zeng, H.; Wang, M. Organic composition tailored perovskite solar cells and light-emitting diodes: Perspectives and advances. *Mater. Today Energy* 2019, *14*, 100338. [CrossRef]

[55] Pulli, E.; Rozzi, E.; Bella, F. Transparent photovoltaic technologies: Current trends towards upscaling. *Energy Convers. Manag.* 2020, *219*, 112982. [CrossRef]

[56] Husain, A.A.F.; Hasan, W.Z.W.; Shafie, S.; Hamidon, M.N.; Pandey, S.S. A review of transparent solar photovoltaic technologies. *Renew. Sustain. Energy Rev.* 2018, *94*, 779–791. [CrossRef]

[57] Bhuvaneswari, P.V.; Velusamy, P.; Babu, R.R.; Babu, S.M.; Ramamurthi, K.; Arivanandhan, M. Effect of fluorine doping on the structural, optical and electrical properties of spray depositedcadmium stannate thin films. *Mater. Sci. Semicond. Proc.* 2013, *16*, 1964–1970. [CrossRef]

[58] Arefi-Khonsari, F.; Bauduin, N.; Donsanti, F.; Amouroux, J. Deposition of transparent conductivetin oxide thin films doped with fluorine by PACVD. *Thin Solid Film.* 2003, *427*, 208–214. [CrossRef]

[59] Elangovan, E.; Ramamurthi, K. Studies on microstructural and electrical properties of spray-deposited fluorine-doped tin oxide thin films from low-cost precursor. *Thin Solid Film.* 2005, *476*, 231–236. [CrossRef]

[60] Elangovan, E.; Ramamurthi, K. A study on low cost-high conducting fluorine and antimony-doped tin oxide thin films. *Appl. Surf. Sci.* 2005, *249*, 183–196. [CrossRef]

[61] Kim, J.H.; Jeon, K.A.; Kim, G.H.; Lee, S.Y. Lee Electrical, structural, and optical properties of ITO thin films prepared at room temperature by pulsed laser deposition. *Appl. Surf. Sci.* 2006, *252*, 4834. [CrossRef]

[62] Martinez, A.I.; Acosta, D.R. Effect of the fluorine content on the structural and electrical properties of SnO2 and ZnO–SnO2 thin films prepared by spray pyrolysis. *Thin Solid Film.* 2005, *483*, 107. [CrossRef]